ARTICLES
https://doi.org/10.1038/s41567-022-01608-w

nature physics

Evidence for spin swapping in an antiferromagnet

Weiwei Lin[1,8], Jiaming He[2,8], Bowen Ma[3], Matthew Matzelle[4], Jinsong Xu[1], John Freeland[5], Yongseong Choi[5], Daniel Haskel[5], Bernardo Barbiellini[6,4], Arun Bansil[4], Gregory A. Fiete[4,7]✉, Jianshi Zhou[2]✉ and C. L. Chien[1]✉

Antiferromagnetic insulators offer strategic advantages in spintronic applications because of their negligible stray fields and ultrafast magnetic dynamics. Control of their magnetization and readout of their magnetic state are essential for these applications but remain challenging. Here we report the electrical detection of room-temperature magnetization switching in the canted antiferromagnetic insulator $LaFeO_3$, capped with a Pt or W overlayer. The observation of a large magneto-thermovoltage with an in-plane temperature gradient suggests that the mechanism is the swapping of spin currents in the antiferromagnet. This effect provides a sensitive electrical probe of the tiny net magnetization in the insulator, which can be manipulated by a magnetic field on the order of 10 mT. Our results highlight a new material class of insulating canted antiferromagnets for spintronics and spin caloritronics and suggests a method for the electrical readout of magnetic signals in an antiferromagnetic insulator.

Electrical detection and control of magnetization orientation are central subjects of study in magnetic materials, spin transport and applications of spintronic devices[1–4]. In ferromagnetic (FM) metals, the magnetization orientation can be switched electrically by using spin-transfer torque and spin–orbit torque techniques. The magnetization orientation can be detected electrically via the anisotropic magnetoresistance, the anomalous Hall effect and the anomalous Nernst effect[5–7]. For ferrimagnetic insulators such as yttrium iron garnet $Y_3Fe_5O_{12}$ (YIG), the longitudinal spin Seebeck effect (LSSE) and the spin Hall magnetoresistance have been employed extensively to reveal the magnetization orientation[8,9]. However, it remains far more challenging to switch and detect the vanishingly small net magnetization of antiferromagnetic (AF) materials. The LSSE has been reported in AF insulators, such as Cr_2O_3 and MnF_2, but only in a large applied magnetic field exceeding the spin-flop field (typically several tesla in magnitude) that induces a canted magnetization in the field direction[10,11]. Subtle quantum effects in some non-collinear AF semimetals, such as the kagome AF Mn_3Sn, allow the anomalous Hall effect and anomalous Nernst effect to reveal a small net magnetization[12,13]. However, it is particularly challenging to accomplish electrical detection of magnetization switching in collinear AF insulators. Evidence of electrical switching of the Néel vector in the AF insulator NiO via an adjacent heavy metal Pt has been reported[14,15], but the origin of the electrical signals used to detect the switching remains debatable[16,17].

In this work, we combine the electrical detection of magnetization switching with the discovery of a large magneto-thermovoltage resulting from a pure spin current in the canted AF $LaFeO_3$/Pt system with an in-plane temperature gradient in a *c*-axis oriented crystal. Since the device with a *c*-axis oriented crystal in our experiment has no out-of-plane signal, our work is qualitatively different from earlier studies where thick samples resulted in an out-of-plane temperature gradient when an in-plane gradient was applied[18]. The voltage signal is comparable in magnitude to that in the YIG/Pt system but unexpected based on the intuition developed for YIG. The crucial difference lies in the nature of the canted magnetism of $LaFeO_3$. In addition, we observe the LSSE in $LaFeO_3$/Pt in the conventional arrangement of a perpendicular temperature gradient for an (*a*,*b*)-axis orientated crystal. $LaFeO_3$/W was also studied in the configurations with an in-plane or perpendicular temperature gradient and produced the sign change in the voltage that is expected from the opposite sign of its spin Hall angle. Together, these results establish a new spin-injection effect, indicating the swapping of spin currents as proposed theoretically[19] in which the spin direction and the direction of the magnon/spin current flow are interchanged. The observation of robust signals in an unconventional temperature gradient and magnetic field configuration may open the door to new applications of magneto-thermal/spin caloritronic effects that exploit the feature of lateral spin transport, which may be important for constrained geometries in device miniaturization[20].

In the devices studied, a spin current is detected with the aid of spin–orbit coupling via the inverse spin Hall effect (ISHE), whereby a spin current is injected from a magnetic insulator into a heavy metal. The spin current is converted into an electrical current, which in turn produces charge accumulation on the boundary of the sample and exhibits an associated electrical potential. Prior studies with such a configuration have been carried out primarily on the combination of Pt and YIG, which has emerged as a standard-bearer in the field[8,9]. However, because of the small number of material combinations in which a strong voltage response is observed from an applied temperature gradient driving the spin current, many possible phenomena still remain experimentally unexplored. With our observation of a strong voltage response to an in-plane temperature gradient, our work is an important step in the direction of widening the collection of established phenomena.

The novel magneto-thermoelectric effects we observe in the $LaFeO_3$/Pt system can be attributed to the low-field magnetization switching of the canted AF insulator $LaFeO_3$ in Fig. 1a. $LaFeO_3$ exhibits G-type magnetic ordering below a Néel temperature of 760 K (refs. [21–23]). Detailed information about the crystal growth and

[1]Department of Physics and Astronomy, Johns Hopkins University, Baltimore, MD, USA. [2]Department of Mechanical Engineering, University of Texas at Austin, Austin, TX, USA. [3]Department of Physics, University of Texas at Austin, Austin, TX, USA. [4]Department of Physics, Northeastern University, Boston, MA, USA. [5]Advanced Photon Source, Argonne National Laboratory, Lemont, IL, USA. [6]School of Engineering Science, LUT University, Lappeenranta, Finland. [7]Department of Physics, Massachusetts Institute of Technology, Cambridge, MA, USA. [8]These authors contributed equally: Weiwei Lin and Jiaming He. ✉e-mail: g.fiete@northeastern.edu; jszhou@mail.utexas.edu; clchien@jhu.edu

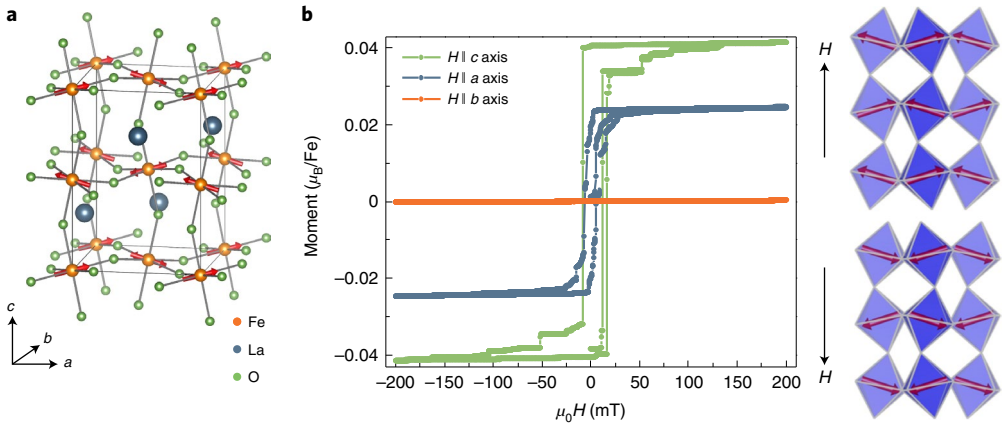

Fig. 1 | Spin structure and magnetization switching of a $LaFeO_3$ crystal. a, The crystal and spin structures of perovskite $LaFeO_3$. The red arrows represent the magnetic moments on Fe^{3+}. The easy axis is along the *a* axis of the cell. Spins are slightly canted to the *c* axis; the canting angle is exaggerated in the plot for demonstration. **b**, The magnetization loop at room temperature of a $LaFeO_3$ crystal with the applied magnetic field along the *a*, *b* and *c* axis. It is difficult to distinguish the *a* axis and the *b* axis from a Laüe pattern because of $a \approx b$. In this case, we label the crystal with (*a*,*b*)-axis orientation. However, the sharply different magnetization in **b** helps assign the crystallographic axes on the crystals we measured. Right: a schematic drawing of the spin orientation for the two different magnetization states with respect to different magnetic field directions along the *c* axis. These two states are responsible for the step-like signal in Fig. 2. The structural models were rendered using VESTA[40].

the characterization is provided in the Supplementary Materials. Figure 1b shows the magnetization in a $LaFeO_3$ crystal with the magnetic field *H* applied along the *a, b* and *c* axes. A spontaneous magnetization is observed when the magnetic field is applied along the *a* axis (the Γ_2 spin structure) and *c* axis (the Γ_4 spin structure), as illustrated in Supplementary Fig. 8. The spin-canting moment with a magnitude of $0.04\mu_B$ (where μ_B is the Bohr magneton) is about 1% of the high-spin Fe^{3+} moment[21,22]. With the expected $5\mu_B$ on Fe^{3+}, the canting angle is approximately 0.52° (ref. [24]). The extremely sharp magnetization switching at the coercive field is inconsistent with domain-wall dynamics[25]. It results from flipping all the spins by 180° (ref. [26]), as illustrated in Fig. 1b. However, when the magnetic field is applied along the *b* axis, there is no detectable spontaneous magnetization or switching, which is consistent with the Γ4 spin structure. The canted spin structure of $LaFeO_3$ and switching behaviour in an external field have consequences for spin injection and underlie our observed unusual magneto-thermovoltage responses. YIG, by contrast, behaves like a normal ferromagnet with negligible magnetocrystalline anisotropy.

For the electrical detection of the magnetization switching in insulating $LaFeO_3$, we deposited a thin (few-nanometre) film of metals showing weak (Cu) or strong (Pt, W) spin–orbit coupling onto polished $LaFeO_3$ by using direct-current (DC) magnetron sputtering at room temperature. We first describe the magneto-thermoelectric effect in (*a*,*b*)-axis oriented $LaFeO_3$ single crystals (3 mm × 3 mm, 0.5 mm thick) in which the canted moment along the *c* axis is in the plane parallel to the interface with a 3-nm-thick Pt overlayer, as illustrated in Fig. 2a. We measured the transverse magneto-thermovoltage in the (*a*,*b*)-axis oriented $LaFeO_3$/Pt with a vertical temperature gradient $\nabla_z T$ (about 10 K mm^{-1}) and an in-plane magnetic field. Figure 2b shows the magnetic loop of the thermovoltage for an in-plane magnetic field applied in various directions within the plane parallel to the Pt layer. The piece-wise constant thermovoltage–magnetic field loops with sharp switching resemble the magnetization loops shown in Figs. 1b and 2f. There is no obvious exchange-bias effect in these loops. This configuration is a standard LSSE geometry with an out-of-plane temperature gradient and an in-plane magnetic field, as in all previous experiments using magnetic insulators such as YIG/Pt[8,9]. However, as shown in Fig. 2c, the angular dependence of the saturated transverse thermovoltage shows a step-like dependence rather than the usual sinusoidal behaviour observed in YIG/Pt.

The step-like dependence indicates that the thermovoltage in $LaFeO_3$/Pt depends only on the canted magnetization, which is along the *c* axis in $LaFeO_3$. The magnetization switching field and the angle of the applied magnetic field follow a $1/|\cos\alpha|$ dependence (Supplementary Fig. 3), with a fitting parameter H_c close to the coercive field obtained from the magnetization measurement. Because the magnetization switching field is at its minimum along the *c* axis, we can easily identify the *c* axis in the (*a*,*b*)-axis oriented $LaFeO_3$, which is about 30° with respect to the *x* direction in the plane (Fig. 2a, dotted line). Furthermore, we also observed the magneto-thermoelectric effect in $LaFeO_3$/W, which exhibits the opposite sign of the voltage relative to $LaFeO_3$/Pt (Supplementary Fig. 4b,e), consistent with the opposite sign of the spin Hall angle in these two heavy metals. In addition, no signal is detected in $LaFeO_3$/Cu (Supplementary Fig. 4b). Together, these observations support the conclusion that the signal is an intrinsic LSSE where a vertical (or out-of-plane) temperature gradient drives a spin current $\mathbf{J}_S$ with spin polarization $\hat{\boldsymbol{\sigma}}$ across the interface into the Pt (W) layer and the thermal voltage is detected via the inverse spin Hall effect (ISHE) with the *y* component of a transverse charge current $\mathbf{J}_c$ (refs. [4,27])

$$\mathbf{J}_c = (2e/\hbar)\,\theta_{SH}\mathbf{J}_S \times \hat{\boldsymbol{\sigma}}, \tag{1}$$

where *e* is the electron charge and θ_{SH} is the spin Hall angle of Pt (W). The transverse magneto-thermoelectric coefficient is $S = V/(d\,\nabla T)$, where *d* is the separation of the two voltage probes. The *S* value of the (*a*,*b*)-axis oriented $LaFeO_3$/Pt is about 0.01 μV K^{-1} for an out-of-plane temperature gradient in the configuration of Fig. 2a. The ratio of the thermovoltage to the canted moment in $LaFeO_3$/Pt is comparable to that of YIG/Pt. When the measurement with the same configuration was applied to a *c*-axis oriented $LaFeO_3$/Pt, no switching signal was detected (Fig. 2e). This is because the net magnetization remains along the *c* axis, parallel to $\mathbf{J}_S$, giving rise to zero ISHE voltage, and the contribution of Γ_2 spin structure to the LSSE is negligible.

Although the *c*-axis oriented crystal shows no switching signal in the standard configuration with the vertical temperature gradient, we made remarkable observations on the *c*-axis oriented crystal

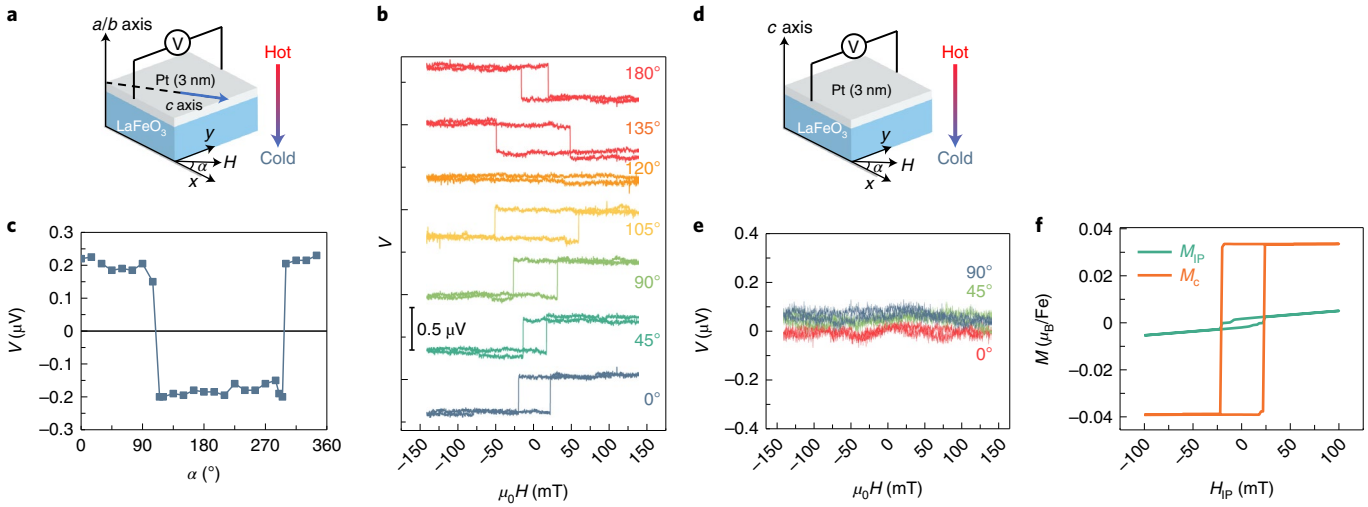

Fig. 2 | Magneto-thermovoltage measurements on $LaFeO_3$/Pt with an out-of-plane temperature gradient. a, Schematic of a transverse thermal voltage measurement in (*a*,*b*)-axis oriented $LaFeO_3$/Pt with an out-of-plane temperature gradient along the *z* direction and an in-plane applied magnetic field. Blue arrow: direction of spontaneous magnetization in $LaFeO_3$. The angle between the *c* axis and the *x* axis is approximately 30°. **b**, Magnetic field dependence of the transverse thermovoltage in (*a*,*b*)-axis oriented $LaFeO_3$/Pt for various in-plane field angles. The voltage for the 120° angle (which is a nearly flat curve) is negative not zero and results because the *c*-axis magnetization remains positive over the magnetic field range shown. **c**, Transverse thermovoltage at magnetic saturation as a function of in-plane field angle. The piece-wise constant form is in stark contrast to what is observed in the YIG/Pt system, which shows a continuous dependence on the magnetic field. **d**, Schematic of a transverse thermal voltage measurement in *c*-axis oriented $LaFeO_3$/Pt with an out-of-plane temperature gradient along the *z* direction and an in-plane applied magnetic field. **e**, Magnetic field dependence of the transverse thermovoltage in *c*-axis oriented $LaFeO_3$/Pt in the configuration of **d**. **f**, Magnetic field dependence of the magnetization of *c*-axis oriented $LaFeO_3$ with in-plane magnetic field by using vector vibrating-sample magnetometry. The magnetization along the in-plane field direction (M_{IP}, green) and along the *c* axis (M_c, perpendicular to the field, orange) were measured simultaneously.

with an in-plane temperature gradient, as illustrated in Fig. 3. An in-plane temperature gradient would naively only generate a spin current parallel to the interface but not produce a voltage signal, yet we obtain a strong, reproducible (across several devices) response. In the configuration of Fig. 3, a 3 nm Pt (W) layer was deposited on a crystal plate with *a* and *b* axes in the plane, a thermal gradient $\nabla_x T$ of 3.3 K mm^{-1} was applied along the *x* direction and a magnetic field was scanned continuously in the *x*–*y* plane and along the *z* axis. Figure 3b shows a large magneto-thermovoltage in the $LaFeO_3$/Pt device. The transverse magneto-thermoelectric coefficient *S* of the *c*-axis oriented $LaFeO_3$/Pt is about 0.15 μV K^{-1} for the in-plane temperature gradient, on the same order of magnitude as the anomalous Nernst coefficient of Fe. Similar to the configuration with the vertical temperature gradient in Fig. 2, the loop of the magneto-thermovoltage versus magnetic field is extremely sensitive to the angle α. A loop with sharp switching is found at α values of 0° and 180°, while an evolution to asymmetric loops is observed between these two angles. These asymmetric loops are in sharp contrast to the symmetric loops centred at zero field seen in Fig. 2. It is also important to note that no switching takes place at $\alpha = 80°$, which is consistent with the assignment of the *b* axis along this direction where no spontaneous magnetization can be obtained in Fig. 1b. Whereas the switching field extracted from Fig. 3b is comparable to the coercive field from the magnetization measurement, the asymmetric loops reflect a strong exchange/bias effect at the interface of $LaFeO_3$ and Pt. Again, the thermovoltage magnitude is independent of the component of spontaneous magnetization along the field direction and exhibits a nearly constant value depending on the canted spin direction as in Fig. 3c. These features are rooted in the spin structure and magnetocrystalline anisotropy of $LaFeO_3$.

The measurement configuration with a magnetic field along the *z* axis also produces sharp switching as shown in Fig. 3d,e. The magneto-thermovoltage reverses with the direction of the temperature gradient (Supplementary Fig. 6). When Pt is replaced by W in Fig. 3d the voltage exhibited a loop as in Fig. 3e but with the opposite polarization (Supplementary Fig. 4e). As Pt and W have opposite sign of the spin Hall angle, these results indicate that the ISHE is a key ingredient to convert the thermally injected spin current into an electric potential in the in-plane thermal gradient configuration. Our results in Fig. 3 are different from those in YIG/Pt, in which there is no magneto-thermovoltage with an in-plane temperature gradient under either in-plane or perpendicular fields[18,28]. In the configuration of Fig. 3d, the temperature gradient, net magnetization and voltage are mutually perpendicular, different from the transverse and the nonlocal spin Seebeck effect, where the temperature gradient, net magnetization and voltage are all in-plane[29]. We stress that, for $\alpha = 0°$ in Fig. 3a, the magnetic field direction and the thermal gradient are parallel. Thus, if the magnetization is aligned along the magnetic field, this vanishing angle is seemingly against the requirement for the magneto-thermovoltage described by equation (1). However, the magnetocrystalline anisotropy of $LaFeO_3$ responsible for the canted moment guarantees that the moment does not continuously follow the field as in YIG. One may suspect that the anomalous Hall effect could create a potential in the configuration of Fig. 3d. To rule out this possibility, we have replaced the thermal gradient with an electric current. No discernible signal has been found (Supplementary Fig. 4l).

We have found magneto-thermovoltage switching in $LaFeO_3$/Pt(W) with two distinct measurement configurations. With a vertical temperature gradient as in the normal LSSE, the magnitude of the thermovoltage from the (*a*,*b*)-axis oriented $LaFeO_3$/Pt is independent of the field direction but changes sign once the canting moment switches, in sharp contrast to the sinusoidal behaviour observed in YIG/Pt. Since the transverse spin Seebeck effect reported in prior magnetic insulator/Pt systems has been attributed to the LSSE due to a component of vertical temperature gradient[18], the observation of the thermovoltage switching with the in-plane temperature gradient in the *c*-oriented $LaFeO_3$/Pt(W) is

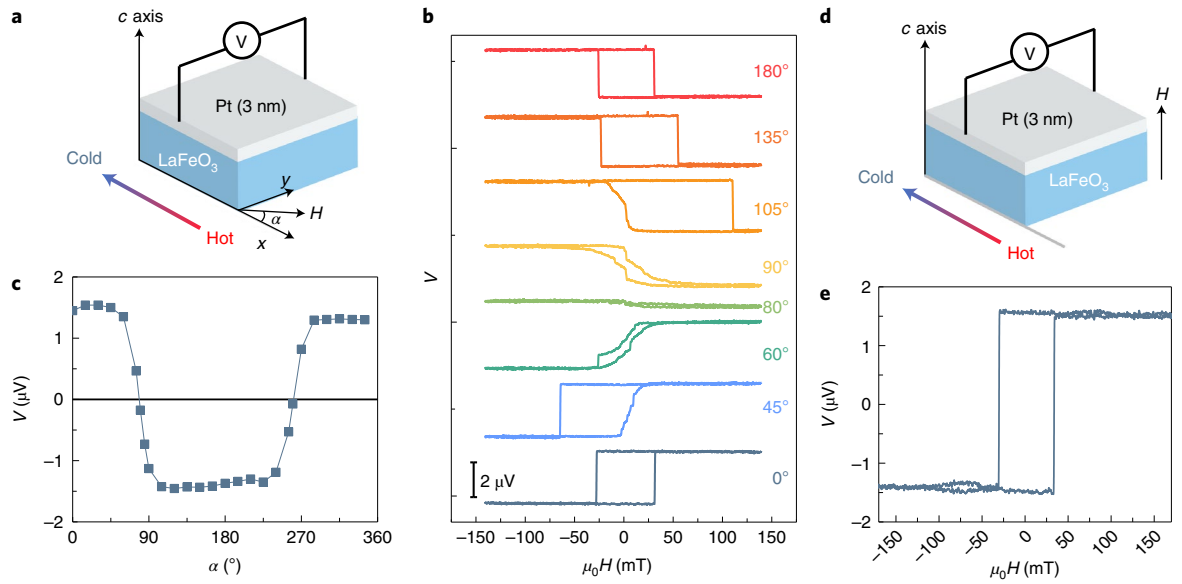

Fig. 3 | Magneto-thermovoltage measurements on the *c*-axis oriented $LaFeO_3$/Pt with an in-plane temperature gradient. a, Schematic of the transverse thermal voltage measurement in *c*-axis oriented $LaFeO_3$/Pt with an in-plane temperature gradient along the *x* direction and an in-plane magnetic field. **b**, Magnetic field dependence of the transverse thermovoltage in *c*-axis oriented $LaFeO_3$/Pt for various in-plane field angles (see Supplementary Fig. 7a,b for the results from 180° to 360°). **c**, Transverse thermovoltage at magnetic saturation as a function of in-plane field angle. **d**, Schematic of transverse thermovoltage measurement in *c*-oriented $LaFeO_3$/Pt with in-plane temperature gradient and magnetic field along *z* direction. **e**, Magnetic field dependence of the transverse thermovoltage from the device in **d**. Such strong and clear signals have not been previously reported in any system with an in-plane temperature gradient.

truly remarkable given that no LSSE can be discerned in this device (Fig. 2e). Evidently, we observe a new intrinsic effect.

To establish the absence of induced magnetic moments due to proximity effects from the $LaFeO_3$ substrate, we have also measured the X-ray magnetic circular dichroism at the Fe $L_{2,3}$ and Pt $L_{2,3}$ edges at room temperature (Supplementary Fig. 7c,d). No detectable magnetic signal from the interface can be observed in $LaFeO_3$/Pt with an applied field of 0.45 T for Pt and 0.4 T for Fe measurements, indicating that both the average magnetization of Fe and the proximity magnetization in Pt are negligibly small (less than $0.03\mu_B$ per Pt atom and $<0.1\mu_B$ per Fe atom). Together, our X-ray magnetic circular dichroism measurements on $LaFeO_3$/Pt as well as the presence of the same unusual magneto-thermoelectric effect in $LaFeO_3$/W and $LaFeO_3$/Cu/Pt (Supplementary Fig. 4f,e) indicate that the observed signal is intrinsic to spin injection from the insulating magnetic structure and does not result from any known charge-current or proximity-induced effects.

The well-established LSSE-type measurement and the interpretation are applicable to the (*a*,*b*)-axis oriented $LaFeO_3$/Pt with a vertical temperature gradient. Note that our LSSE results in the intrinsically canted AF $LaFeO_3$ are different from those reported in the high field-induced canting (spin flop) in the AF $Cu_2V_2O_7$ (ref. [30]) and $DyFeO_3$ (ref. [31]). No magneto-thermovoltage for a measurement with an in-plane temperature gradient and any direction of applied magnetic field is expected for the configuration in Fig. 3a,d based on the LSSE mechanism for a magnetic moment that continuously follows the direction of the applied field, such as occurs in YIG[18,28]. Indeed, no pure spin-injection thermovoltage has been observed in any FM or AF insulator under an in-plane temperature gradient. Besides the LSSE mechanism, we also considered a situation where a vertical spin current injects from $LaFeO_3$ via the magnon Nernst effect as $J_z^x = \alpha_{zx}^x \nabla_x T$, where J_z^x is the *x*-polarized spin current along the *z* direction and α_{zx}^x is the magnon Nernst response of the in-plane temperature gradient. However, the *a*,*b*-plane mirror symmetry of $LaFeO_3$ imposes $\alpha_{zx}^x = 0$ and rules out a possible bulk contribution to the thermal voltage from the magnon Nernst effect (Supplementary Information). An in-plane temperature gradient creates a magnon current in the *x* direction with spin polarization along the *z* direction, giving rise to a voltage in the *y* direction. This might be explained by an interfacial electron–magnon interaction where thermal magnons scatter with itinerant electrons at the Pt interface during the propagation along the *x* direction and transfer momenta and spin angular momenta to the electrons, inducing a *z*-polarized spin current J_x^z. This spin current at the Pt interface then generates a charge current (voltage) along the *y* direction by ISHE. However, this generic effect has never been reported in other magnetic insulator–heavy metal heterostructures and cannot easily explain the evolution of the signal between 0° and 180° in Fig. 3b.

We propose a spin-torque swapping effect to explain the in-plane temperature gradient results. Because of the mirror symmetry breaking and spin–orbit coupling at the interface, an interfacial Dzyaloshinskii–Moriya interaction (DMI) can arise in the $LaFeO_3$/Pt heterostructure. Similar to the torques arising f rom the electron flow in a magnetic two-dimensional electron gas with Rashba spin–orbit coupling, when the thermal gradient drives a magnon current $\mathbf{j}_m$ near the interface, the DMI produces an effective field-like torque $\boldsymbol{\tau}_{FL} \propto \mathbf{m} \times (\hat{\mathbf{z}} \times \mathbf{j}_m)$ and a damping-like torque $\boldsymbol{\tau}_{DL} \propto \mathbf{m} \times [(\hat{\mathbf{z}} \times \mathbf{j}_m) \times \mathbf{m}]$[32–34], where $\hat{\mathbf{z}}$ is normal to the interface and $\mathbf{m}$ is the canted moment (Fig. 4). The interchange of directions of the magnon flow and spin index can arise from magnon–magnon or magnon–phonon scattering in the presence of spin–orbit coupling.

As $LaFeO_3$ shows a near degeneracy between the Γ_2 and Γ_4 magnetic configurations[35], the damping-like torque $\boldsymbol{\tau}_{DL}$ mediated by the magnon flow can reorient the interfacial spin ordering from Γ_4 to Γ_2 with a canted moment along the *a* axis, and the changed angular momentum is transferred into Pt/W as an *a*-axis-polarized spin current J_z^a by the interfacial electron–magnon interaction. As shown in Supplementary Fig. 4e, by the ISHE of the heavy metal, this injected spin current is detected as a thermal voltage with opposite signs in

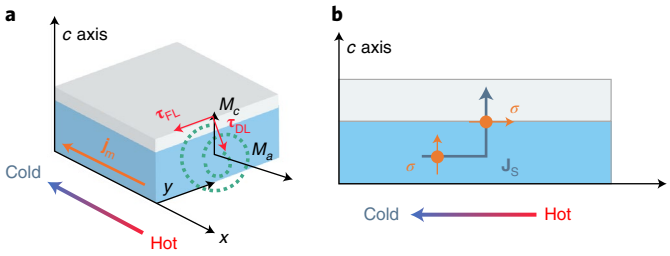

Fig. 4 | Schematic of the spin swapping mechanism at the interface of a *c*-axis oriented $LaFeO_3$ crystal and a heavy metal. a, Schematic of the spin-torque swapping effect in *c*-axis oriented $LaFeO_3$/Pt with an in-plane temperature gradient along the *x* direction. The magnon current $\mathbf{j}_m$ is along the temperature gradient (the magnonic spin current is in the opposite direction to the magnon because it carries spin −1). The dotted line shows the trajectory of the magnetic moment. $\boldsymbol{\tau}_{DL}$ ($\boldsymbol{\tau}_{FL}$) is the damping-like (field-like) spin torque induced by the interfacial DMI which contributes to swapping the net magnetic moment M_c of Γ_4 to an in-plane moment M_a of Γ_2. The *x* component of M_a accompanied by a *z* component of spin-torque-induced spin current then contributes to a detectable voltage along the *y* direction by the ISHE. **b**, Schematic of a 90° rotation of the spin index and the transformation of an in-plane magnon current to an out-of-plane spin current.

Pt and W due to the opposite signs of the spin Hall angle in Pt and W. When the out-of-plane magnetic field flips, both the *c*-oriented canted moment **m** and the magnon current $\mathbf{j}_m$ will flip their sign, leading to a re-oriented moment along the negative *a* axis direction and a negative thermal voltage (Fig. 3e and Supplementary Fig. 4e). When the field is in-plane, the canted moment from the original Γ_4 state and $\mathbf{j}_m$ as well as the induced torques will not be affected by the field[36], while the Zeeman effect from the magnetic field can flip the re-oriented canted moment in a Γ_2 state (Supplementary Fig. 8). These two effects will compete with each other when the in-plane field flips. If we attribute the unswitched thermovoltage at an 80° angle in Fig. 3b as arising from the magnetic field lying along the *b* axis, then one cannot flip the Γ_2 or Γ_4 canted moment. Thus, the large exchange bias near 80° (see 45° and 105° in Fig. 3b) can be explained by the exchange coupling at the Γ_4–Γ_2 domain wall competing against weak Zeeman coupling[37,38]. In addition, the gradually reversed thermal voltage curve around zero field at 80° reflects a Γ_4–Γ_2 spin reorientation instead of a magnetic-field-induced sharp switching. On the other hand, with an out-of-plane thermal gradient, $\hat{\mathbf{z}} \times \mathbf{j}_m = 0$, thus the thermal voltage will not be affected by the DMI torques and only shows square loops without any notable exchange-bias effect in Fig. 2. Such a spin-torque effect provides a consistent interpretation of our experimental results and relies on the specific spin structure and magnetic anisotropy of $LaFeO_3$, which are quite distinct from YIG or any other previously studied material. This explains the absence of a voltage signal from spin injection for an in-plane temperature gradient in prior work. The hallmark of this process (Fig. 4, right) is that the spin index rotates 90° when an in-plane magnon current (mediated by interfacial DMI torques) transforms to an out-of-plane spin current. Such a 'spin-swapping' signal is not expected from the transverse spin Seebeck effect, nonlocal spin Seebeck effect or thermal spin drag[18,39]. The mechanism of a spin structure transition at the interface of $LaFeO_3$/Pt(W) under an in-plane temperature gradient may open a new direction of study for spin caloritronic effects and will certainly spur further experimental and theoretical investigations. We hope to widen their scope through the introduction of a new material class for study.

Online content

Any methods, additional references, Nature Research reporting summaries, source data, extended data, supplementary information, acknowledgements, peer review information; details of author contributions and competing interests; and statements of data and code availability are available at https://doi.org/10.1038/s41567-022-01608-w.

Received: 22 July 2021; Accepted: 7 April 2022;
Published online: 16 May 2022

References

1. Hirohata, A. et al. Review on spintronics: principles and device applications. *J. Magn. Magn. Mater.* **509**, 166711 (2020).
2. Manchon, A. et al. Current-induced spin–orbit torques in ferromagnetic and antiferromagnetic systems. *Rev. Mod. Phys.* **91**, 035004 (2019).
3. Baltz, V. et al. Antiferromagnetic spintronics. *Rev. Mod. Phys.* **90**, 015005 (2018).
4. Sinova, J., Valenzuela, S. O., Wunderlich, J., Back, C. H. & Jungwirth, T. Spin Hall effects. *Rev. Mod. Phys.* **87**, 1213–1260 (2015).
5. McGuire, T. & Potter, R. Anisotropic magnetoresistance in ferromagnetic 3d alloys. *IEEE Trans. Magn.* **11**, 1018–1038 (1975).
6. Pugh, E. M. & Rostoker, N. Hall effect in ferromagnetic materials. *Rev. Mod. Phys.* **25**, 151–157 (1953).
7. Smith, A. W. The Hall effect and the Nernst effect in magnetic alloys. *Phys. Rev.* **17**, 23–37 (1921).
8. Uchida, K. et al. Observation of longitudinal spin-Seebeck effect in magnetic insulators. *Appl. Phys. Lett.* **97**, 172505 (2010).
9. Uchida, K. et al. Thermoelectric generation based on spin Seebeck effects. *Proc. IEEE* **104**, 1946–1973 (2016).
10. Seki, S. et al. Thermal generation of spin current in an antiferromagnet. *Phys. Rev. Lett.* **115**, 266601 (2015).
11. Wu, S. M. et al. Antiferromagnetic spin Seebeck effect. *Phys. Rev. Lett.* **116**, 097204 (2016).
12. Nakatsuji, S., Kiyohara, N. & Higo, T. Large anomalous Hall effect in a non-collinear antiferromagnet at room temperature. *Nature* **527**, 212–215 (2015).
13. Ikhlas, M. et al. Large anomalous Nernst effect at room temperature in a chiral antiferromagnet. *Nat. Phys.* **13**, 1085–1090 (2017).
14. Chen, X. Z. et al. Antidamping-torque-induced switching in biaxial antiferromagnetic insulators. *Phys. Rev. Lett.* **120**, 207204 (2018).
15. Moriyama, T., Oda, K., Ohkochi, T., Kimata, M. & Ono, T. Spin torque control of antiferromagnetic moments in NiO. *Sci. Rep.* **8**, 14167 (2018).
16. Chiang, C. C., Huang, S. Y., Qu, D., Wu, P. H. & Chien, C. L. Absence of evidence of electrical switching of the antiferromagnetic Néel vector. *Phys. Rev. Lett.* **123**, 227203 (2019).
17. Churikova, A. et al. Non-magnetic origin of spin Hall magnetoresistance-like signals in Pt films and epitaxial NiO/Pt bilayers. *Appl. Phys. Lett.* **116**, 022410 (2020).
18. Meier, D. et al. Longitudinal spin Seebeck effect contribution in transverse spin Seebeck effect experiments in Pt/YIG and Pt/NFO. *Nat. Commun.* **6**, 8211 (2015).
19. Lifshits, M. B. & Dyakonov, M. I. Swapping spin currents: interchanging spin and flow directions. *Phys. Rev. Lett.* **103**, 186601 (2009).
20. Yu, H., Brechet, S. D. & Ansermet, J.-P. Spin caloritronics, origin and outlook. *Phys. Lett. A* **381**, 825–837 (2017).
21. Koehler, W. C. & Wollan, E. O. Neutron-diffraction study of the magnetic properties of perovskite-like compounds $LaBO_3$. *J. Phys. Chem. Solids* **2**, 100–106 (1957).
22. Treves, D. Magnetic studies of some orthoferrites. *Phys. Rev.* **125**, 1843–1853 (1962).
23. White, R. L. Review of recent work on the magnetic and spectroscopic properties of the rare-earth orthoferrites. *J. Appl. Phys.* **40**, 1061–1069 (1969).
24. Treves, D. Studies on orthoferrites at the Weizmann Institute of Science. *J. Appl. Phys.* **36**, 1033–1039 (1965).
25. Reich, S., Shtrikman, S. & Treves, D. Angular variation of coercivity in orthoferrite single crystals. *J. Appl. Phys.* **36**, 140–141 (1965).
26. Zhou, J. S., Marshall, L. G., Li, Z. Y., Li, X. & He, J. M. Weak ferromagnetism in perovskite oxides. *Phys. Rev. B* **102**, 104420 (2020).
27. Saitoh, E., Ueda, M., Miyajima, H. & Tatara, G. Conversion of spin current into charge current at room temperature: inverse spin-Hall effect. *Appl. Phys. Lett.* **88**, 182509 (2006).
28. Kikkawa, T. et al. Longitudinal spin Seebeck effect free from the proximity Nernst effect. *Phys. Rev. Lett.* **110**, 067207 (2013).
29. Tikhonov, K. S., Sinova, J. & Finkel'stein, A. M. Spectral non-uniform temperature and non-local heat transfer in the spin Seebeck effect. *Nat. Commun.* **4**, 1945 (2013).
30. Shiomi, Y. et al. Spin Seebeck effect in the polar antiferromagnet $Cu_2V_2O_7$. *Phys. Rev. B* **96**, 180414 (2017).
31. Hoogeboom, G. R. et al. Magnetic order of Dy^{3+} and Fe3+ moments in antiferromagnetic $DyFeO_3$ probed by spin Hall magnetoresistance and spin Seebeck effect. *Phys. Rev. B* **103**, 134406 (2021).

32. Manchon, A., Ndiaye, P. B., Moon, J.-H., Lee, H.-W. & Lee, K.-J. Magnon-mediated Dzyaloshinskii–Moriya torque in homogeneous ferromagnets. *Phys. Rev. B* **90**, 224403 (2014).
33. Pauyac, C. O., Chshiev, M., Manchon, A. & Nikolaev, S. A. Spin Hall and spin swapping torques in diffusive ferromagnets. *Phys. Rev. Lett.* **120**, 176802 (2018).
34. Saidaoui, H. B. M. & Manchon, A. Spin-swapping transport and torques in ultrathin magnetic bilayers. *Phys. Rev. Lett.* **117**, 036601 (2016).
35. Mao, A. J., Tian, H., Kuang, X. Y., Jia, J. W. & Chai, J. S. Structural phase transition and spin reorientation of $LaFeO_3$ films under epitaxial strain. *RSC Adv.* **6**, 100526–100531 (2016).
36. Kovalev, A. A. & Zyuzin, V. Spin torque and Nernst effects in Dzyaloshinskii–Moriya ferromagnets. *Phys. Rev. B* **93**, 161106 (2016).
37. Scholl, A. et al. Observation of antiferromagnetic domains in epitaxial thin films. *Science* **287**, 1014–1016 (2000).
38. Hallsteinsen, I. et al. Magnetic domain configuration of (111)-oriented $LaFeO_3$ epitaxial thin films. *APL Mater.* **5**, 086107 (2017).
39. Avci, C. O. et al. Nonlocal detection of out-of-plane magnetization in a magnetic insulator by thermal spin drag. *Phys. Rev. Lett.* **124**, 027701 (2020).
40. Momma, K. & Izumi, F. VESTA 3 for three-dimensional visualization of crystal, volumetric and morphology data. *J. Appl. Crystallogr.* **44**, 1272–1276 (2011).

Methods

Crystal growth and initial characterizations. Single crystals of $LaFeO_3$ were grown by the floating zone technique with an image furnace (NEC SC-M35HD). A starting ceramic rod of $LaFeO_3$ was prepared by solid-state reaction; La_2O_3 (99.99%, Alfa Aesar) and Fe_2O_3 (99.99%, Alfa Aesar) were thoroughly mixed in a molar ratio of 1:1 and calcined at 1250 °C. The crystal growth was carried out with continuous air flow, and the growth speed was around 8 mm h^{-1}. The obtained single crystal is black in colour with a shiny surface. The phase purity of the obtained $LaFeO_3$ was confirmed by powder X-ray diffraction analysis. The structure of $LaFeO_3$ is in space group *Pbnm* (no. 62) with lattice parameters of $a = 5.566(2)$ Å, $b = 5.554(3)$ Å and $c = 7.861(2)$ Å. The crystal orientation as well as the crystal quality were determined by Laüe back-reflection. The oriented crystals were polished by using lapping films (30 to 0.1 μm) to obtain a flat, shiny surface. After polishing, Raman spectra were taken with a confocal Renishaw inVia Raman microscope using a laser with wavelength of 532 nm and power of 10 mW. X-ray photoelectron spectra of the polished surface were taken in the vacuum chamber of a Kratos system, and also of an insitu cleaved crystal for comparison. Magnetization measurements were carried out in a vibrating-sample magnetometer by using a Physical Property Measurement System from Quantum Design.

Device fabrication and measurements. A layer of Pt or W heavy metal was deposited on the polished crystal pellets by DC magnetron sputtering at room temperature. The deposition rate of the metal layer was calibrated by the film thickness measured by X-ray reflectivity. The magneto-thermovoltage measurements were performed using a nanovoltmeter and a rotatable electromagnet. The $LaFeO_3$/Pt(W) devices were attached to a resistive heater as the hot side and a Cu plate as the cold side. The temperatures of the sample were checked by the resistance of the Pt stripes deposited on the $LaFeO_3$ crystal. In a typical measurement with a vertical temperature gradient, the temperature difference along the direction of the sample thickness is about 5 K (temperature gradient of about 10 K mm^{-1}), whereas it is about 10 K (temperature gradient of about 3.3 K mm^{-1}) across the crystal plate in the configuration with an in-plane temperature gradient.

First-principles calculations. First-principles calculations within the density functional theory framework were carried out on $LaFeO_3$ using the pseudopotential projector-augmented wave method[41] implemented in the Vienna ab initio simulation package[42,43] with the Perdew–Burke–Ernzerhof implementation of the exchange correlation functional[44]. A plane-wave basis set cutoff of 600 eV was chosen, and the atomic positions and lattice parameters of the $LaFeO_3$ unit cell were relaxed from experimental values until the forces on each atom were below 0.008 eV $Å^{-1}$. Self-consistency was concluded when the energy difference between subsequent electronic calculations was less than 0.1 μeV. Calculations were done on a Γ-centred grid of $12 \times 12 \times 8$ reciprocal-space points. Typically, these calculations include a Hubbard U term to better model the effects of electronic correlation. We find that calculations without the term correctly lead to an antiferromagnetic insulator ground state.

The initial relaxation assumes collinear magnetism and is performed with the conjugate-gradient algorithm implemented in the Vienna ab initio simulation package. However, after optimizing the atomic positions and lattice parameters, we allow a non-collinear magnetic structure and include spin–orbit coupling self-consistently[45]. Previous non-collinear density functional theory calculations have been performed for $LaFeO_3$ (ref. [46]). However, unlike previous works, the present calculations have been performed fully self-consistently. To find the correct ground state, we performed calculations with different initial conditions. We initialized the Fe magnetic moments along different crystallographic axes in each of the calculations. The calculated non-collinear magnetic orders are consistent with other theoretical studies and agree with experimental findings[47].

Data availability

Source data are available. Additional data supporting the findings of this study are available from the corresponding author upon request. Source data are provided with this paper.

References

41. Kresse, G. & Joubert, D. From ultrasoft pseudopotentials to the projector augmented-wave method. *Phys. Rev. B* **59**, 1758–1775 (1999).
42. Kresse, G. & Furthmüller, J. Efficient iterative schemes for ab initio total-energy calculations using a plane-wave basis set. *Phys. Rev. B* **54**, 11169–11186 (1996).
43. Kresse, G. & Hafner, J. Ab initio molecular dynamics for open-shell transition metals. *Phys. Rev. B* **48**, 13115–13118 (1993).
44. Perdew, J. P., Burke, K. & Ernzerhof, M. Generalized gradient approximation made simple. *Phys. Rev. Lett.* **77**, 3865–3868 (1996).
45. Steiner, S., Khmelevskyi, S., Marsmann, M. & Kresse, G. Calculation of the magnetic anisotropy with projected-augmented-wave methodology and the case study of disordered $Fe_{1-x}Co_x$ alloys. *Phys. Rev. B* **93**, 224425 (2016).
46. Weingart, C., Spaldin, N. & Bousquet, E. Noncollinear magnetism and single-ion anisotropy in multiferroic perovskites. *Phys. Rev. B* **86**, 094413 (2012).
47. Bousquet, E. & Cano, A. Non-collinear magnetism in multiferroic perovskites. *J. Phys. Condens. Matter* **28**, 123001 (2016).

Acknowledgements

We acknowledge support from US National Science Foundation DMREF grants DMR-1729555, DMR-1729588 and DMR-1949701. G.A.F. acknowledges additional funding from DMR-2114825. The work of M.M., B.B. and A.B. was supported by US Department of Energy, Office of Science, Basic Energy Sciences grant no. DE-SC0019275 and benefitted from Northeastern University's Advanced Scientific Computation Center and the National Energy Research Scientific Computing Center through Department of Energy grant no. DE-AC02-05CH11231. This research used resources of the Advanced Photon Source, a Department of Energy Office of Science User Facility operated by Argonne National Laboratory under contract no. DE-AC02-06CH11357.

Author contributions

J.Z., W.L., G.A.F. and C.L.C. conceived the research plan. J.M.H. and J.Z. grew the $LaFeO_3$ crystals, performed crystal characterizations, and oriented and polished the crystal pellets. W.L. and J.X. fabricated the devices and performed the magneto-thermovoltage measurements. B.M. and G.A.F. carried out the modelling and theoretical work. M.M., B.B. and A.B. performed the density functional theory calculations. J.F., Y.C. and D.H. performed the X-ray magnetic circular dichroism measurements. All co-authors contributed to the data analysis and writing of the manuscript.

Competing interests

The authors declare no competing interests.

Additional information

Supplementary information The online version contains supplementary material available at https://doi.org/10.1038/s41567-022-01608-w.

Correspondence and requests for materials should be addressed to Gregory A. Fiete, Jianshi Zhou or C. L. Chien.

Peer review information *Nature Physics* thanks Günter Reiss and the other, anonymous, reviewer(s) for their contribution to the peer review of this work.